DOE/ER/13987--74

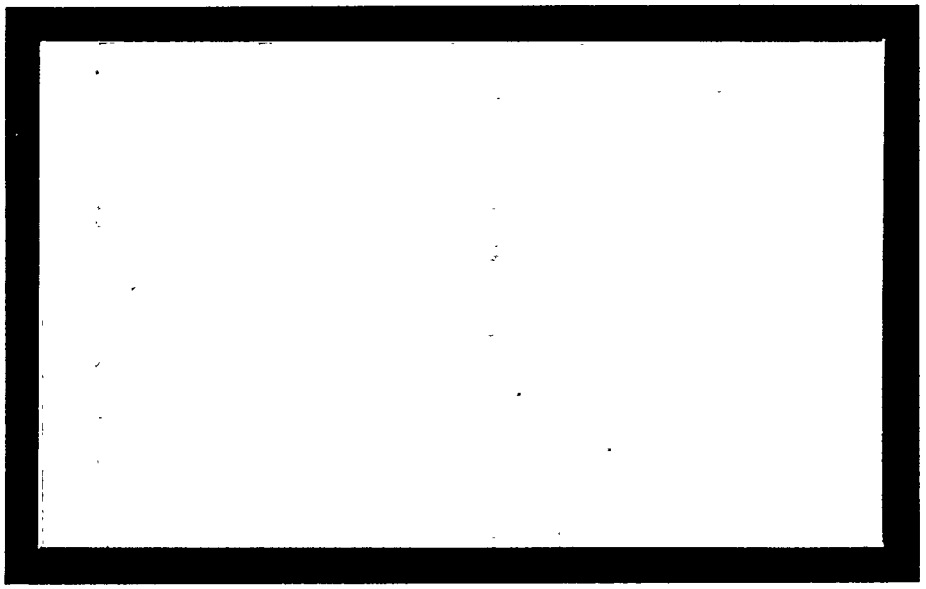

CENTER FOR MATERIALS RESEARCH

STANFORD UNIVERSITY • STANFORD, CALIFORNIA

The Board of Trustees of the
Leland Stanford Junior University
Center for Materials Research
Stanford, California 94305-4045
Santa Clara, 12th Congressional District

Progress Report
on

GROWTH OF HIGH T_c SUPERCONDUCTING FIBERS USING A MINIATURIZED LASER-HEATED FLOAT ZONE PROCESS

for the period
Contract No. DE-FG03-89ER-13987
January 1, 1992 through December 31, 1992

Submitted to
Division of Advanced Energy Projects
Office of Basic Energy Sciences
ER-16, GTN
Department of Energy
Washington, DC 20545
CMR-92-1

DISCLAIMER

Principal Investigator:

Robert S. Feigelson, Professor (Res.)
Center for Materials Research
Stanford, California 94305-4045
(415) 723-4007

December 1992

MASTER COPY KEEP THIS COPY FOR REPRODUCTION PURPOSES

REPORT DOCUMENTATION PAGE

Form Approved
OMB No. 0704-0188

1. AGENCY USE ONLY (Leave blank)	2. REPORT DATE	3. REPORT TYPE AND DATES COVERED
	Dec. 31, 1992	Progress Report

4. TITLE AND SUBTITLE
Growth of High T_c Superconducting Fibers Using a Miniaturized Laser-Heated Float Zone Process

5. FUNDING NUMBERS
DE-FG03-89ER-13987

6. AUTHOR(S)
Robert S. Feigelson
Roger K. Route
Robert C. DeMattei

7. PERFORMING ORGANIZATION NAME(S) AND ADDRESS(ES)
Center for Materials Research
Stanford University
Stanford, CA 94305-4045

8. PERFORMING ORGANIZATION REPORT NUMBER
CMR-92-1
SPO #6462

9. SPONSORING / MONITORING AGENCY NAME(S) AND ADDRESS(ES)
Office of Basic Energy Sciences, ER-16
Department of Energy
Germantown, MD 20545

10. SPONSORING / MONITORING AGENCY REPORT NUMBER
FTR

11. SUPPLEMENTARY NOTES
The view, opinions and/or findings contained in this report are those of the author(s) and should not be construed as an official Department of position, policy, or decision, unless so designated by other documentation.

12a. DISTRIBUTION / AVAILABILITY STATEMENT
Approved for public release; distribution unlimited.

12b. DISTRIBUTION CODE

13. ABSTRACT *(Maximum 200 words)*

This report covers the research done on "Growth of High Tc Superconducting Fibers using a Miniaturized Laser-Heated Float Zone Process" during the 12 months from Jan. 1, 1992 until Dec. 31, 1992. The major part of the work focused on phase relations and kinetics in the Bi_2O_3-SrO-CaO-CuO (BSCCO) system. By analyzing the crystal and melt composition, and the growth temperature of the float-zone samples, new data was obtained on the phase relationships. These results were shown to form a subset of solid solubility ranges reported by other investigators and was typical of the data available from other flux growth experiments.

These experiments resulted in the development of a technique for the growth of long, single-phase 2212 samples. This was highly depended on starting material composition with $Bi_{2.1}Sr_{1.8}Ca_{1.1}Cu_2O_y$ being the most successful.

Examination of the single phase 2212 growth interfaces was used to characterize the crystal/melt equilibrium conditions. These studies showed that 2212 crystal solidify from Bi_2O_3-rich and SrO-poor melts.

Increasing melt concentrations of bismuth and cooper oxide increased the growth temperature. The sum of the bismuth and copper oxide in the crystals was invariant leading to the conclusion that the segregation of bismuth and copper oxide is interdependent.

Work also proceeded on the new LHPG growth station.

14. SUBJECT TERMS
High T_c Superconductors, BSCCO, BiSrCaCuO, Superconducting Fibers/Ceramics, LHPG High T_c. Phase Equilibria

15. NUMBER OF PAGES
36

16. PRICE CODE

17. SECURITY CLASSIFICATION OF REPORT	18. SECURITY CLASSIFICATION OF THIS PAGE	19. SECURITY CLASSIFICATION OF ABSTRACT	20. LIMITATION OF ABSTRACT
UNCLASSIFIED	UNCLASSIFIED	UNCLASSIFIED	UL

GROWTH OF HIGH T_c SUPERCONDUCTING FIBERS USING A MINIATURIZED LASER-HEATED FLOAT ZONE PROCESS

TABLE OF CONTENTS

GROWTH OF HIGH T_c SUPERCONDUCTING FIBERS USING A MINIATURIZED LASER-HEATED FLOAT ZONE PROCESS

I. INTRODUCTION

This program (initially planned for three years) has been devoted to establishing the viability of the laser-heated pedestal growth (LHPG) method for the preparation of wire of the high T_c superconductor $Bi_2Sr_2CaCu_2O_8$. This material not only exhibits a high superconducting transition temperature and high critical current densities, but also has better thermodynamic properties (low volatility in particular) than other high Tc superconducting materials. In particular this material has become one of the most attractive materials for superconducting wire applications.

This program had as its main goals 1) finding the most appropriate starting compositions capable of producing long lengths of wire with uniform structure and composition, high superconducting transition temperatures, and critical current densities, 2) maximizing the growth velocity to enhance the economic viability of the growth method and 3) determining the maximum length of fiber which can be produced. To address these issues, we have made 1) an in-depth study of the thermodynamic and kinetic factors which affect growth rates and the properties of the fibers produced, 2) designed and started construction of an advanced fiber growth system which will permit better control of system parameters, and 3) developed of techniques to enhance fiber throughput via increased growth velocity. Most of this program was suscessfully completed by the end of the initial three year period.

At the conclusion of the third year (December 16, 1991) we found it necessary to request a six month no-cost extension (to June 14, 1992) due to delays in obtaining the CO_2 laser necessary for our advanced fiber growth system. The sealed waveguide, grating stabilized CO_2 laser ordered from Laser Photonics Inc, in Florida did not meet specifications and so after a 19 month time period we initiated a search for another laser. This delayed the completion of the growth system and the final crystal growth experiments.

During this reporting period we finally located a new company promising a laser with even better specifications, but they could not deliver before the original no-cost extension expired, and so on May 18, 1992 we requested and

were granted another six month no-cost extension (to December 31, 1992) to permit the completion of this project.

Results during the period January 15, 1989 to December 31, 1991 are summarized in Progress Reports CMR 89-3 dated April 1989, CMR 90-8 dated November 1990, and CMR 91-1 dated December 1991

II. PROGRESS TO DATE

This report covers the fourth year of this program. Most of the materials research work had been completed during the previous three year period. During this last 12 month period, as covered in this fourth year report, the emphasis has been on 1) finishing up some of the phase studies on the Bi-Sr-Ca-Cu-O system, 2) obtaining the appropriate laser for the new advanced fiber growth system, and 3) completing construction of the growth system.

A. PHASE RELATIONS AND KINETICS IN THE Bi_2O_3-SrO-CaO-CuO SYSTEM

The critical importance of starting material quality in the high T_c superconductors was made amply clear during the early phases of this program. Multi-phase source rods containing unreacted grains of a size comparable to the source rod diameter will lead to significant changes in melt and fiber composition during growth, and to growth instabilities. To facilitate our knowledge of the LHPG solidification behavior of a complicated incongruently melting material such as the BSCCO superconductor, we studied the kinetic and thermodynamic effects present during LHPG fiber growth in a simplier model system. The CaO-Al_2O_3 system was chosen for this purpose. This work was completed last year (see CMR 91- 1) and the comparative BSCCO phase studies were completed this year

Wavelength dispersive spectroscopic (WDS) analysis, using a JEOL 733 Scanning Electron Microscope, was used to evaluate both the phase content and the compositional profiles in the 2212 crystalline material, quenched melts, source rods. The chemical compositions of various 10 micron diameter regions were obtained using electrons accelerated with 15 kV. Standardization was performed using, wollastonite ($CaSiO_3$), metallic bismuth and copper, and strontium titanate ($SrTiO_3$) standards. Consecutive measurements were

reproducible to approximately 2 atomic % of the total content of each element (for example, a bismuth stoichiometry of 2.00 would be reproducible to approximately ±0.04). The data obtained from the CaO-Al_2O_3 solidification study was in good agreement with the established CaO-Al_2O_3 phase diagrams and crystallization theory. This study also clearly showed that useful phase equilibrium information on incongruently melting materials can be extracted from these miniaturized float-zone growth experiments and could be appropriately used to determine the relevant features fo the phase relations in the BSCCO system.

The relationship between crystal and melt composition during the float-zone growth of $Bi_2Sr_2CaCu_2O_{8+d}$ was studied by comparison with the Ca aluminate results discussed in the previous year's progress report. We began by making a study and summary of the limited phase equilibrium information available in the literature. It covered the 2212 solid solubility ranges, as determined by Ono, [1] Golden et al., [2] and Hong et al., [3] as well as the limited crystal and melt composition data which may be determined from other crystal growth studies. The variation in segregation coefficient of the various components in the superconductor with crystal composition was evaluated.

The results of this study are compared with the literature results and with those of Lombardo's recent bulk crystallization study. [4] The trends found did not generally depend on the experimental method employed, thus all available data was considered.

1. Phase equilibria

(a.) Solid solubility and solid/solid equilibria

$Bi_2(Sr,Ca)_3Cu_2O_{8+d}$ (2212) is one of three distinct superconducting phases in the Bi_2O_3-SrO-CaO-CuO (BSCCO) system. [5-7] This phase is much easier to crystallize from the melt than the higher-T_c (~110° K) 2223 superconductor, which exists in equilibrium with its melt only over a very narrow temperature range. The solubility range of the 2212 phase, has been explored in many studies, among them references. [1-3,8,9] There are some significant discrepancies in the interpretation of their x-ray diffraction results, for example, differences in the identities of the crystal structures of some of the solid phases formed. This is not surprising since many of the BSCCO phases have complex x-ray patterns with strong similarities and exist over unexplored composition regions. In part, these differences may be explained by the type of experimental techniques used. In the current studies, the only concern was the composition of minority-phase inclusions and not their crystal structures.

The complex quaternary BSCCO system contains a number of phase fields which contain the 2212 compound. Schweizer et al., [8] for instance, reported equilibrium between the 2212 phase and three other solid phases in four different phase fields. This is illustrated in Figure 1, which summarizes the results of Schweizer et al. as they apply to 2212 phase stability. Their detailed results, unfortunately, do not include the melt-solid phase equilibria regions of most relevance to crystal growth processors. On the other hand, the solid-state reaction techniques used were useful in identifying regions of the phase fields which were either partially or completely molten at a particular temperature. However, the segregation of various components during solidification make this data unreliable for identifying specific "melt-solid" relationships.

The solid-state reaction experiments performed by Ono [1] produced the most detailed description of the 2212 solid solubility range available in the early stages of our study. In Ono's study single-phase, polycrystalline samples of a variety of compositions were made. The compositions which produced single phase (within the limits of his analytical techniques) samples were of the form: $Bi_2(Bi,Sr,Ca)_3Cu_2O_{8+d}$, which implied that to stabilize the 2212 structure, excess Bi is required on the Sr and Ca sites.

Ono's samples were prepared by reacting CuO, Bi_2O_3, $SrCO_3$, and $CaCO_3$ powders at elevated temperatures. The final reaction steps occurred in air at temperatures between 865 and 885°C. This is quite close to the temperatures at which the various 2212 compositions are known to melt.

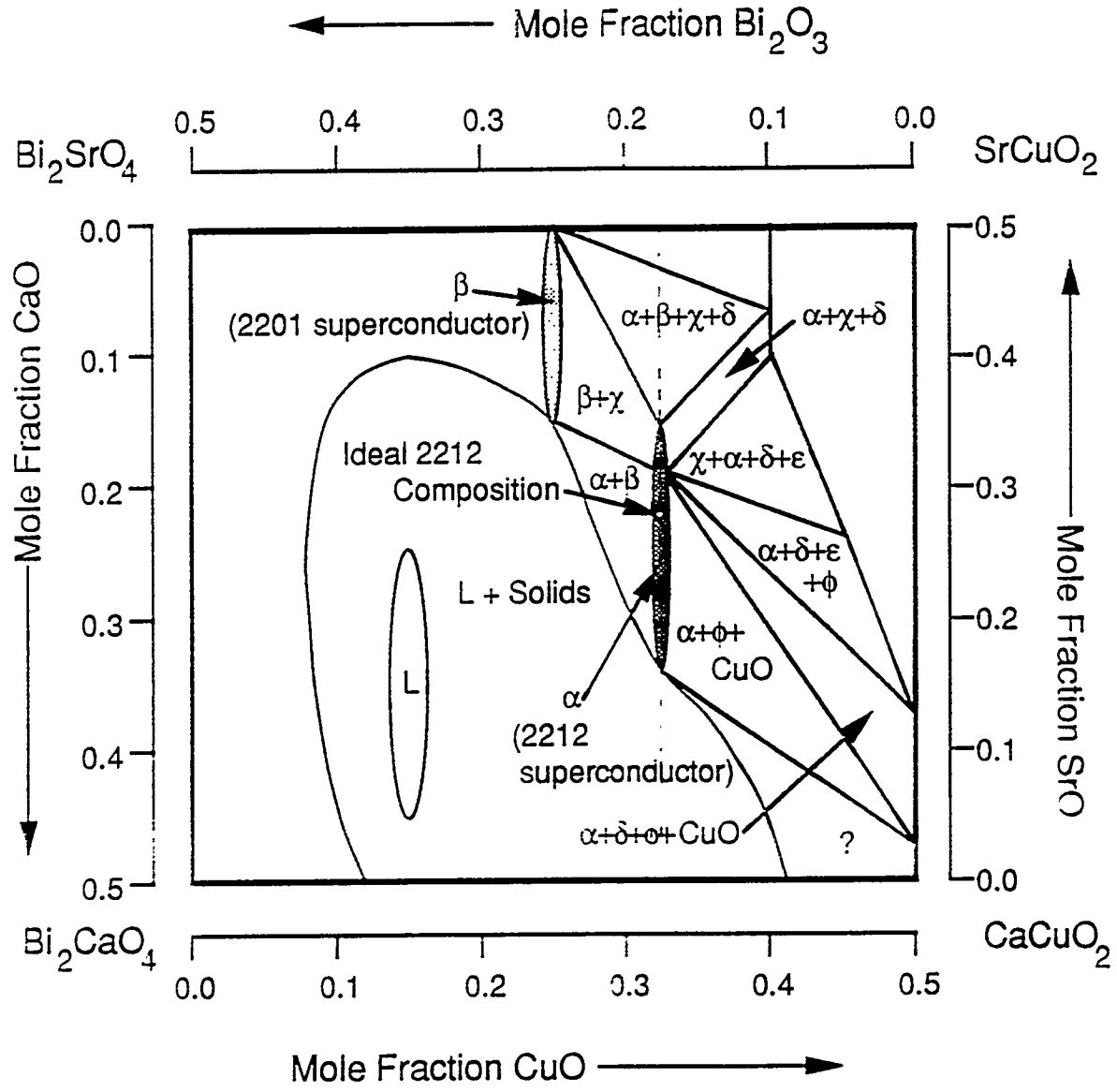

Figure 1: Phase coexistence at 830°C in planar cut of BSCCO compositional tetrahedron. From information and diagrams in Schweizer et al. [8] L represents the presence of an oxide melt. The Greek letters indicate the presence of the solid solutions with structures: α-$Bi_2(Sr,Ca)_3Cu_2O_y$, β-$Bi_2Sr_2CuO_y$, γ-$Bi_4Sr_8Cu_5O_y$, δ-$Sr_{14}Cu_{24}O_y$, ε-$Bi_3Sr_4Ca_3O_y$, and ϕ-Sr_2CuO_y.

Figure 2 illustrates 2212 solid solubility ranges reported by Ono, [1] and others. Note that the compositions are all significantly Bi_2O_3-rich compared to the stoichiometric "2212" composition. Using a standard normalization (the sum of the metal ion coefficients equals 7.0), the total bismuth content of Ono's single-phase samples varied from 2.05 to 2.20. In addition, the calcium-to-strontium ratio in these same samples varied between 0.3 and 1.2.

Figure (2) shows a planar cut though the Bi_2O_3-SrO-CaO-CuO compositional tetrahedron. The relative orientation of this plane within the tetrahedron is shown, along with that of the plane examined by Schweizer et al. [8] in Figure 3(a).

The Ono solid solubility range is also shown in the pseudo-ternary representation of $Bi_X(Sr,Ca)_YCu_ZO_n$ in Figure 4. This figure reduces the BSCCO compositional tetrahedron to a ternary representation by viewing the alkaline earth oxides (SrO and CaO) as indistinguishable. This is often a useful representation because these oxides are chemically similar and the compounds in the BSCCO system often display extensive (Sr,Ca)O intersolubility.

In Figure 4, the Ono solubility range is confined to the Cu=2 line. This was a result of Ono's experimental design. He presumed that compositions of the form $Bi_2(Bi,Sr,Ca)_3Cu_2O_8$ would completely describe the solubility range of the 2212 solid. His experiments were thus not designed to test the copper oxide solubility.

Lee et al. [9] used x-ray diffraction to examine samples which had been first equilibrated at 850 and 900°C, then quenched in liquid nitrogen. They only considered samples with a Sr:Ca ratio of 2:1. At 850°C they found that the 2212 phase can be in equilibrium with a variety of other compounds.

Golden et al. [2] also examined the solubility range of 2212, but by an unusual technique. Rather than producing samples by the solid-state reaction of powders, they formed superconducting thin films of various compositions on MgO substrates. This was accomplished by melting organic precursors. The coated substrates were then subjected to extended heat-treatment at sub-solidus temperatures. Figures 2 and 4 illustrate the compositional range of the single-phase thin films produced by this technique. This range of compositions is treated here as their "solid solubility" range, and they are noticeably more Bi_2O_3-rich and SrO-poor than the other solubility regions discussed.

The data given by Schweizer et al. [8] on the compositional ranges for the 2201 and 2212 superconductors (Figure 1) was obtained at a temperature of 830°C. This study provided limited data on the compositional range of the melt in this isothermal section.

Most recently, Hong et al. [3] identified three phases present at 860°C along the binary joins between 2212 and the other compounds that they believed were present in the BSCCO system at elevated temperatures. They identified the limits of the 2212 solid solubility range by measuring the compositions of the $Bi_2(Sr,Ca)_3Cu_2O_{8+d}$ grains in their multi-phase samples. This solid solubility range is shown in Figures 2 and 4.

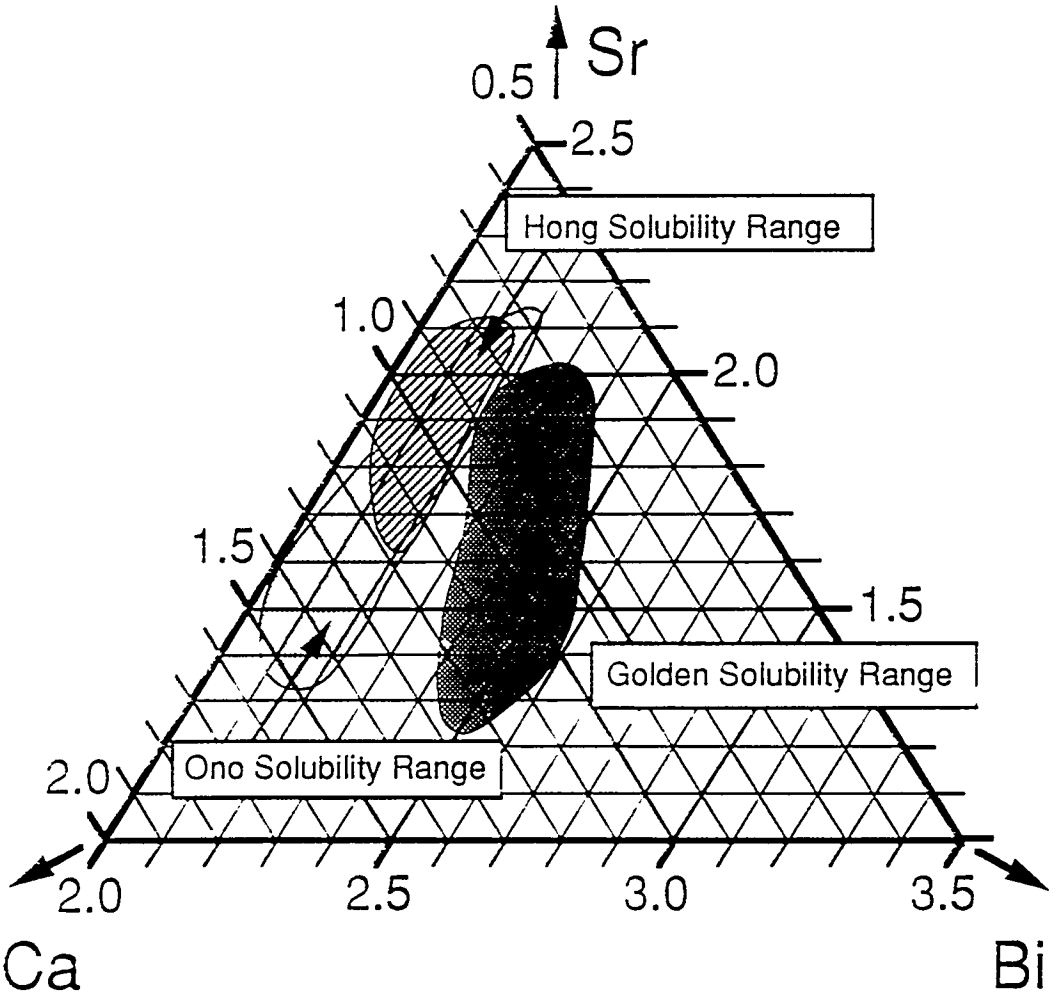

Figure 2: Ternary representation of compositions $Bi_xSr_yCa_zCu_2O_{8+d}$. This shows the solid solubility ranges determined by Ono [1] and Golden et al.[2] and Hong et al. [3]

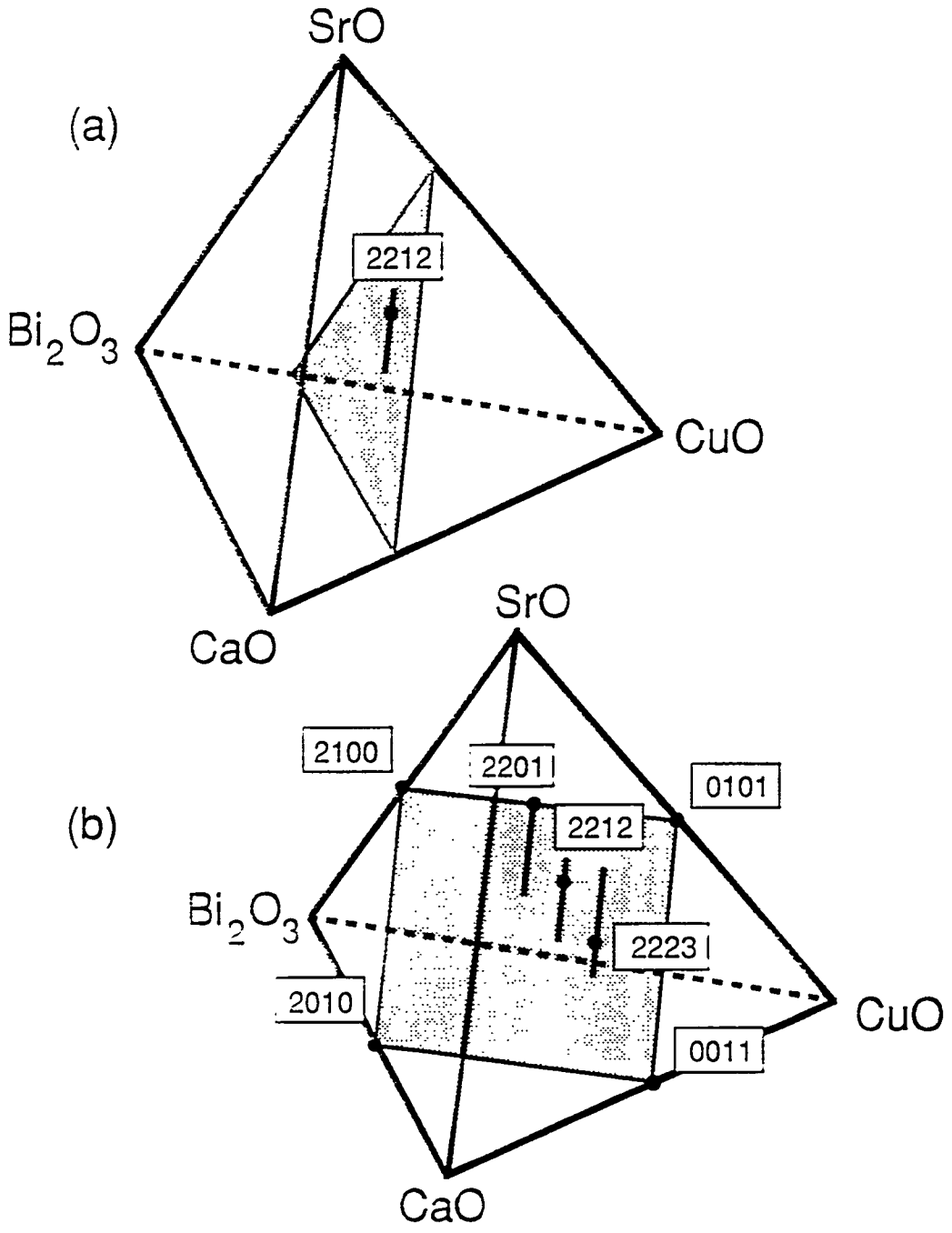

Figure 3 Plane sections of the BSCCO tetrahedron showing the relative orientations of: (a) the Cu=2, iso-copper plane and (b) the planar section analyzed by Schweizer et al. [8] The 2212 phase is located roughly at the intersection of these two planes. The Schweizer plane contains all three superconducting compounds in the BSCCO system.

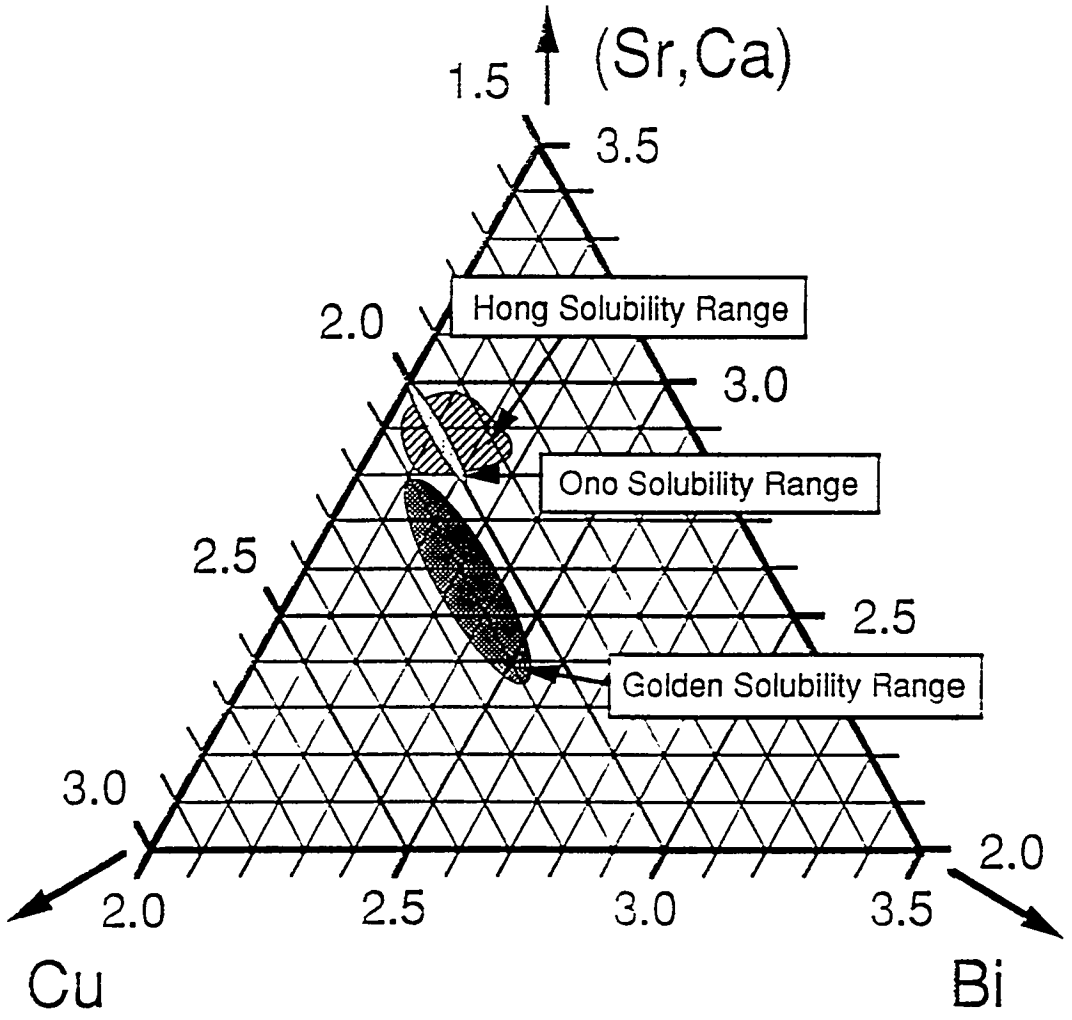

Figure 4: Ternary $Bi_x(Sr,Ca)_yCu_zO_n$ representation which shows the solid solubility ranges determined by Ono [1] and Golden et al. [2] and Hong et al. [3]

The technique Hong et al. [3] used in their study provided accurate information on only a few key data points, but these points were carefully chosen. Unfortunately, they did not include information on the solid (2212)-melt equilibria. As one can observe from Figure 1, the data of Schweizer et al. shows that the applicable melt compositions do not lie along the binary joins investigated in Hong et al.'s study . Consequently, they missed a large portion of the CaO-rich 2212 phase found by Ono.

(b.) Melt/solid equilibria

Many studies have been concerned with the growth of 2212 crystals from oxide melts, [10-12,6,7,9,13-16] including several [11,12,15-17] which employed the float-zone technique. Their results confirmed the existence of a "2212 + liquid" phase field. The resulting melt and crystal compositions reported in these studies are summarized in Table 1. The compositions listed in parentheses have been normalized to Bi+Sr+Ca+Cu=7.0. Typically, crystals of the nominal composition $Bi_{2.1}Sr_{1.9}Ca_{1.0}Cu_2O_y$ can be grown in the 850 to 890°C temperature range. The melt compositions reported were Bi_2O_3-rich and SrO-poor when compared with the crystal compositions growing from them.

Table 1: Melt and Crystal Composition Data from Literature

Reference	Crystal Composition	Melt Composition	Crystallization Temperature
[2]	2.10: 1.94: 0.88: 2.07		
[6]	~2.0: 1.5: 1.5: 2.0		885°C
[19]	2.2: 1.8 1.0: 2.0 2.2: 2.1: 0.7: 2.0 2.3: 1.2: 05: 2.0		
[9]	2.2: 1.8: 1.0: 2.0	2.4: 1.5: 1.0: 1.8 (2.5: 1.55: 1.05: 1.9)	
[13]	2.11: 2.11: 0.89: 2.00 (2.05: 2.05: 0.86: 1.94)		
[14]	2.18: 1.87: 0.99: 1.97	2.6: 1.9: 1.0 2.6 (2.25: 1.65: 0.85: 2.25)	
[12]	2.5: 2.0: 1.0: 2.2 (2.3: 1.8: 0.9: 2.0)	2.80: 1.61: 0.91: 1.68	850° C (in 1 atm O_2)
[16]	2.13: 1.95: 0.75: 2.0 (2.18: 2.00: 1.01: 2.05)		
	2.1: 1.9: 0.9: 2.0 (2.13: 1.93: 1.02: 2.03)	2.2: 1.6: 0.85: 1.8 (2.4: 1.75: 0.92: 1.95)	

Golden et al. [2] provided additional information on the "2212 + liquid" phase field. They determined the melting temperatures of their thin films by optical and differential thermal analysis. Their compositions and the associated melting temperatures are listed in Table 2. The melting temperatures in this study were significantly lower than those reported in other studies and were consistent with their unusually Bi_2O_3 and CuO-rich crystal compositions.

Table 2: Experimental Compositions and Melting Temperatures

Crystal Composition		Melting Temperature
2.10: 1.71: 0.85: 2	(2.21: 1.80: 0.89: 2.10)	835°C
2.16: 1.53: 0.95: 2	(2.28: 1.61: 1.00: 2.11)	830
2.38: 1.57: 0.92: 2	(2.43: 1.66: 0.97: 2.11)	830
2.25: 1.45: 0.96: 2	(2.36: 1.52: 1.01: 2.10)	835
2.38: 1.33: 0.94: 2	(2.51: 1.40: 1.00: 2.11)	810
2.35: 1.40: 0.96: 2	(2.45: 1.46: 1.04: 2.09)	810
2.45: 1.38: 0.94: 2	(2.53: 1.43: 0.97: 2.07)	800
2.20: 1.92: 0.66: 2	(2.27: 1.98: 0.68: 2.06)	840
2.19: 1.68: 0.67: 2	(2.34: 1.80: 0.72: 2.14)	840
2.18: 1.89: 0.73: 2	(2.24: 1.95: 0.75: 2.06)	845
2.10: 1.81: 0.83: 2	(2.18: 1.87: 0.86: 2.08)	845
2.24: 1.32: 1.12: 2	(2.35: 1.38: 1.17: 2.10)	820
2.34: 1.15: 1.20: 2	(2.45: 1.20: 1.26: 2.09)	785

As yet, no one has found a unique composition which is congruently-melting. It is more difficult to prepare large high quality crystals of incongruently-melting compounds due to segregation phenomena at the growth interface. To avoid this problem, they must be crystallized from melt compositions which differ from the solidifying solid and, therefore, at relatively slow growth rates. By examining the segregation coefficients for each of the major components in these 2212 float-zone growth studies, compositions were

found which crystallize with minimum segregation. These results are discussed in later sections.

2. Crystallization Studies

(a.) Mass transport in BSCCO melts

Figure 5 shows a schematic drawing for the float-zone growth of an incongruently-melting solid, along with the temperature (Figure 5(a)) and compositional (Figure 5(b)) profiles which would result. The degree of solute buildup and depletion at the solid/liquid interfaces depend on growth rate.

The compositional variations within the boundary layer can be determined by the relative rates of reaction at the interfaces and solute transport across the molten zone. Unless the growth rate is infinitely slow, one would not expect the complete elimination of compositional variation. Any molten zone from which crystallization is occurring at a finite rate thus contains nonsymmetric compositional profiles which drive any diffusive transport which occurs in the melt.

Figures 6 (a-c) show SEM micrographs of the cross sections of three 2212 samples quenched during the stable growth period. Each sample exhibits a different type of structure and phase content: (a) contains the higher temperature (HT) phase, (b) is a single-phase sample and (c) contains the lower temperature (LT) phase.

The major goal of this study was to produce inclusion-free 2212 crystals, i.e. the case shown in Figure 6(b). The sample shown in Figure 6(a) contains not only 2212 grains (grey) but also dark refractory oxide inclusions which had a low Bi_2O_3 content. Figure 6(c) also contains Bi_2O_3-rich fine-grained inclusions running parallel to the growth direction. In all cases, however, the solid formed from a Bi_2O_3-rich molten zone.

Since Bi_2O_3 acts as a flux for many refractory oxides, [18] it was not surprising to find the Bi_2O_3 acting as a solvent during the growth of 2212 crystals. It was also consistent with the results of prior 2212 crystallization studies which are listed in Table 1. It was also not surprising to see the formation of Sr-Ca-Cu oxides, as these are much higher melting temperature phases.

It can be seen from Figures 6 (a) and (c) and Figure 7 that a mushy (melt+solid) zone exists at the melting interfaces. The appearance of these zones showed that a solute-depleted regions existed in the melt at these

interface regardless of whether multiphase or single phase source rods were used.

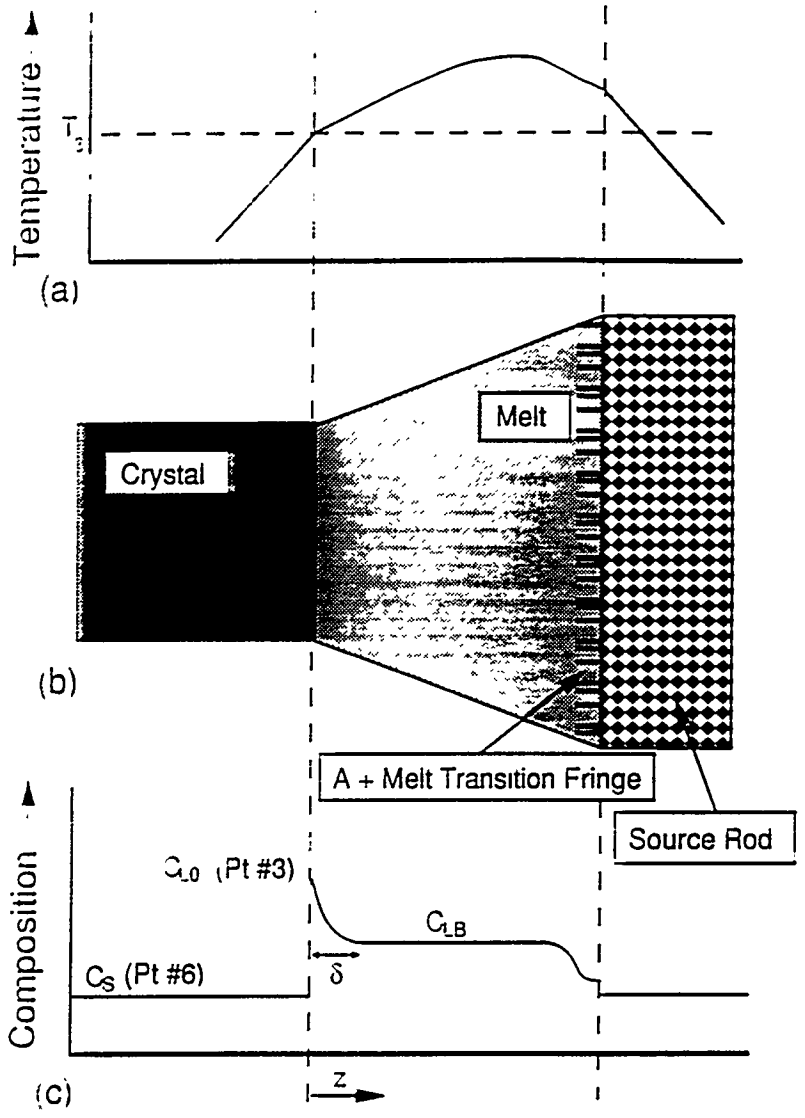

Figure 5: Representative (a) temperature and (c) composition profiles in the melt and solids near the molten zone. These are shown along the growth direction, which has been rotated 90° from its experimental orientation.

(a) (b) (c)

Figure 6: Composite electron micrographs of quenched sample cross-sections (diameters ~ 600 mm) grown with feedstock compositions (a) W, (b) Y, and (c) V.

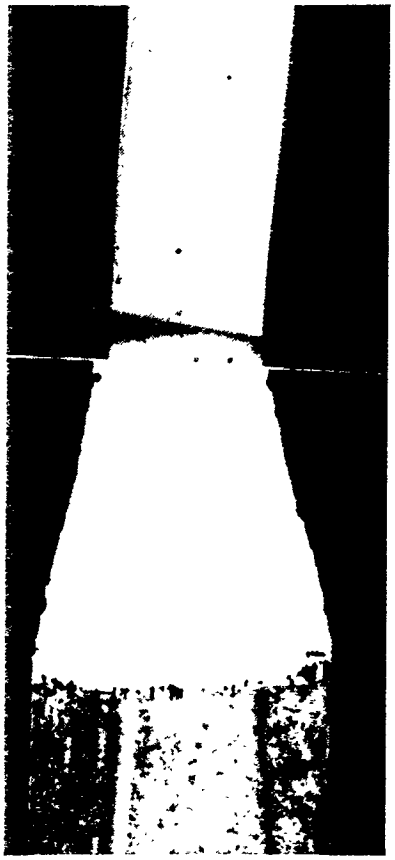

Figure 7: Internal cross section of quenched $Bi_2(Sr,Ca)_3Cu_2O_{8+d}$ growth front. This sample was crystallized from a single-phase source rod of composition Y and is approximately 500 mm diameter.

(b.) Influence of starting material composition

An important goal of this study was to determine a suitable starting material composition to use for the growth of long 2212 single crystals. This was accomplished using 850 mm diameter multiphase source rods prepared as described in a previous section.

Table 3 gives the different starting material compositions investigated in this study and the resulting microstructures produced after steady-state growth had been achieved. These compositions are plotted along with the Ono's [1] solubility data in Figure 8.

Table 3: Effects of Starting Material Composition

Starting Material	Composition (Bi: Sr: Ca: Cu)				Comments
Y	2.10:	1.80:	1.10:	2.00	Best composition for stable, single phase growth.
P	2.20:	1.50:	1.30:	2.00	Produced stable, single phase (SP) growth.
Z	2.10:	1.60:	1.30:	2.00	Produced stable, SP growth.
E	2.05:	1.60:	1.35:	2.00	Produced stable, SP growth.
A	2.15	2.10	0.75	2.00	Produced stable, SP growth.
B	2.17	2.13	0.70	2.00	Produced stable, SP growth.
X	2.15:	1.80:	1.05:	2.00	Produced substantial lengths of SP growth.
R	2.05:	1.95:	1.00:	2.00	Produced substantial lengths of SP growth.
U	2.00:	2.00:	1.00:	2.00	Nominal composition. Produced some SP growth.
V	2.00:	1.60:	1.40:	2.00	Variant of nominal composition. Did not produce SP growth.
W	2.20:	1.80:	1.00:	2.00	Produced short lengths of SP growth.
Q	2.40:	1.50:	1.10:	2.00	Produced SP growth from the initial melt, but did not support extended, SP growth.

Stable, single phase 2212 material was successfully produced using the starting compositions designated Y, Z, E, P, A, and B. Of these, composition Y was identified as particularly dependable. It allowed a relatively easy transition from the early, multi-phase growth stage to steady-state growth with relatively little component segregation. Samples grown with this starting material composition also had relatively high T_cs.

On the other hand, it was found that compositions E and P exhibited a more complex transient behavior before single-phase growth could be achieved and the samples grown from starting material Z had lower T_cs. Compositions A and B were not extensively studied. They did, however, produce stable, single-phase material, which was SrO- and CuO-rich. These compositions exhibited relatively low Bi_2O_3 segregation and are, therefore, promising candidates for future work.

When starting materials of compositions U or R were used, multi-phase growth persisted for 2-3 hours before single-phase growth was observed. Attempts to grow more than 3-5 mm single-phase material were, however, not successful due to a periodic disruption of the growth process leading to the incorporation of refractory oxide inclusions. Thus, while several millimeter lengths of single-phase sample were often generated using U or R composition starting material, their growth was prone to catastrophic breakdown. Note that compositions R and U both contain insufficient Bi_2O_3 to lie within the Ono solubility region in Figure 8.

Composition V is also Bi_2O_3-poor compared to the compositions in the Ono solubility region. Single-phase growth was never achieved with starting material of composition V. Instead, samples were consistently multiphase. The refractory oxide inclusions do not have a high electrical conductivity and can form insulating barriers between the 2212 grains. These samples did not conduct well along their lengths, unless the electrical contacts were connected to a single 2212 grain.

Starting materials of compositions X, W, and Q produced single phase growth very soon after the growth process began, but this was followed by multiphase growth with LT inclusions. Typically, these inclusions were first observed as trapped melt at the 2212 grain boundaries. In later stages, they were also observed to form within the 2212 grains. Thus, at the lower growth temperatures, it appears that constitutional supercooling is still a problem even for growth at 4.8 mm/hr in a steep (~1000°/cm) temperature gradient.

The duration of the single-phase steady-state growth regime varied for compositions X, W, and Q. Inclusions were not apparent in samples produced using X until after 5-8 mm of single-phase material had been grown. This composition was initially thought to be suitable for stable, single-phase growth, but the growth of long samples, however, showed that it was not. Compositions W and Q, on the other hand, provided more extreme examples of

transient, single-phase growth. These compositions produced <2.5 mm of single phase material.

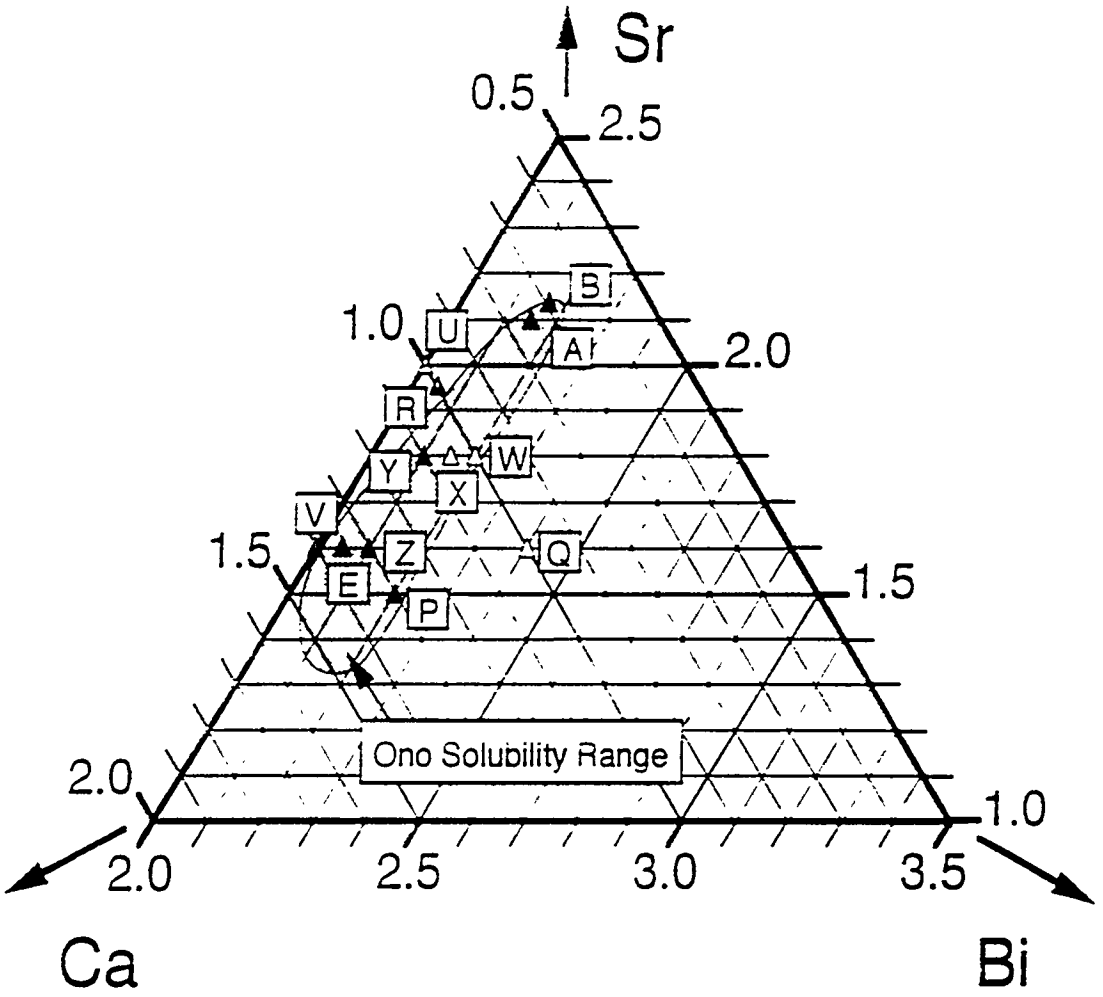

Figure 8: Ternary representation of starting material compositions $Bi_XSr_YCa_ZCu_2O_{8+d}$ (where X+Y+Z=5.0) and their position relative to Ono's $Bi_2(Sr,Ca)_3Cu_2O_{8+d}$ solid solubility [10] region.

(c.) Crystal/melt equilibria at the growth front

The compositions of a variety of crystals grown in this study are listed in Table 4. They are accompanied by 1) the letter designating of the starting material composition, 2) the composition of the molten zone, 3) their growth temperatures, and 4) the solid phases found at the growth interface.

Many of these samples were quenched during an early stages of growth and, therefore, the composition of the growing crystal differed from that of the

starting material because the melt composition had not yet reached its steady-state value. For this reason, growth was terminated only after the molten zone geometry and surface appearance remained unchanged for at least 15 minutes. Using this procedure assured that the phases present in the quenched molten zones were representative of true steady-state equilibrium. The composition values given in Table 4, therefore, give a good picture of the ("2212" + melt) phase field.

3. Characterization

(a.) Solid solubility ranges

The compositional data given in Table 4 are plotted in Figures 9 and 10, alongside the Ono [1], Golden et al.[2] and Hong et al.[3] solubility data. In Figure 9, the crystal compositions is represented as triangles and the melt compositions as circles. Both sets of symbols are projected on the $Bi_XSr_YCa_ZCu_2O_{8+d}$ plane. Figure 10 shows the same information, but using the form $Bi_X(Sr,Ca)_YCu_ZO_n$. The gray-level in these symbols indicates the type of solid phases present at the growth interface. Single-phase regions are indicated by the white symbols. HT and LT phases are represented by black and gray symbols, respectively. Related compositions at each interface are connected by tie-lines in Figures 9 and 10. These are represented by a solid line when an approximately planar growth interface was observed, otherwise they are represented as a dashed line.

Several observations can be made concerning the compositional data plotted in Figure 9. First, the observed crystal compositions correspond closely to those in the Ono solubility range. The melt compositions are all Bi-rich and Sr-poor with respect to both the Ono solid solubility values. These can be expressed by the segregation coefficients ($k=C_S/C_L$). The segregation coefficient measured for Bi_2O_3 was <1.0 and >1.0 for SrO. The CaO segregation coefficient varied about both sides of 1.0.

The melt compositions found in this study corresponded closely to the Golden solubility values. The Golden solubility range thus corresponds more to the liquidus, rather than the solidus values of the 2212 phase.

TABLE 4: Data Obtained from Composite Samples

Trial	Source	Crystal Comp (Bi: Sr: Ca: Cu)				Melt Comp (Bi: Sr: Ca: Cu)				Temp	Inclusions
#1	(B)	2.16	2.05	0.77	2.02	2.40	1.81	0.68	2.11*	-	None
2	(Y)	2.16	1.77	1.10	1.97	2.44	1.47	1.09	2.00	>875°C	None
3	(X)	2.23	1.76	1.06	1.95	2.36	1.58	1.02	2.04	890	None
4	(E)	2.17	1.61	1.20	2.01	2.40	1.40	1.22	1.98	890	None
5	(Z)	2.17	1.56	1.24	2.02	2.40	1.26	1.16	2.18*	880	None
6	(P)	2.17	1.56	1.27	2.01	2.35	1.21	1.20	2.25*	880	None
7	(A)	2.15	2.00	0.80	2.05	2.22	1.63	0.69	2.46*	-	None
8	(Y)	2.22	1.77	0.99	2.02	2.39	1.52	1.02	2.06*	>875	None
9	(E)	2.11	1.55	1.31	2.02	2.37	1.38	1.29	1.95*	>875	None
10	(Z)	2.19	1.59	1.23	1.97	2.52	1.28	1.19	2.02	875	None
11	(YY)	2.21	1.70	1.11	1.97	2.52	1.41	1.10	1.97	870	None
12	(YY)	2.13	1.76	1.10	2.01	2.47	1.47	1.03	2.03	865	None
13	(V)	2.17	1.60	1.20	2.03	2.49	1.18	1.25	2.08*	>875	Ca_2CuO_3
14	(U)	2.17	1.92	0.89	2.01	2.54	1.73	0.90	1.83*	900	CaO
15	(R)	2.14	1.92	0.96	1.98	2.20	1.67	0.95	2.18*	890	Sr_2CuO_3?
16	(ZZ)	2.26	1.41	1.31	2.02	2.72	1.16	1.28	1.83*	865	Nonplanar
17	(QQQ)	2.21	1.59	1.20	2.01	2.76	1.26	1.06	1.93*	845	Nonplanar
18	(X)	2.19	1.77	1.04	2.00	2.63	1.45	1.04	1.88*	840	Bi_2O_3-rich
19	(W)	2.21	1.76	1.02	2.01	2.63	1.40	1.03	1.94*	840	Bi_2O_3-rich
20	(QQQ)	2.28	1.58	1.18	1.96	2.91	1.09	1.24	1.76*	<850	Bi_2O_3-rich

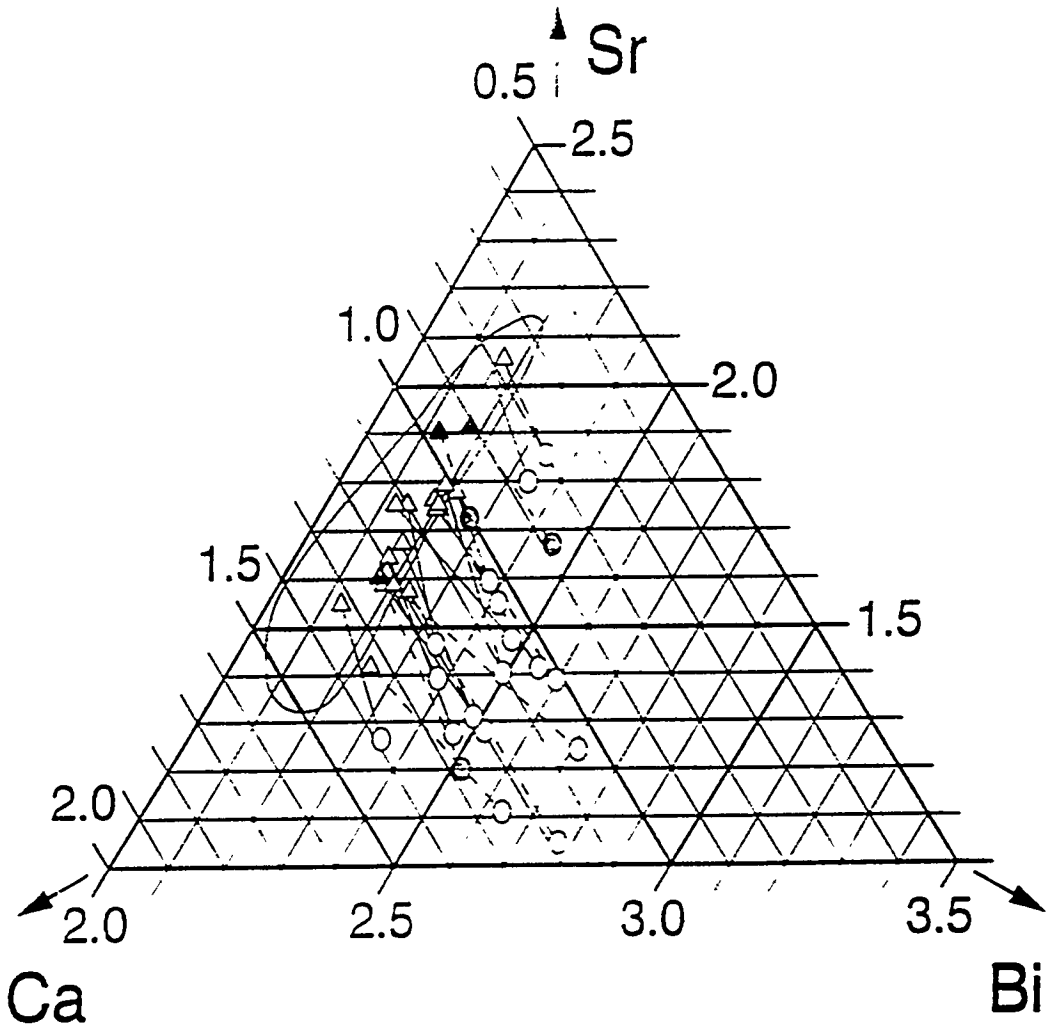

Figure 9: Ternary projection of crystal and melt compositions on the $Bi_xSr_yCa_zCu_2O_{8+d}$ planar section. Crystal compositions are shown as triangles, while melt compositions are shown as circles. Symbols which are white indicate ~planar, single-phase crystallization fronts, while grey symbols represent cases of non-planar solidification fronts. Lines connect the various crystal compositions to their respective melt compositions.

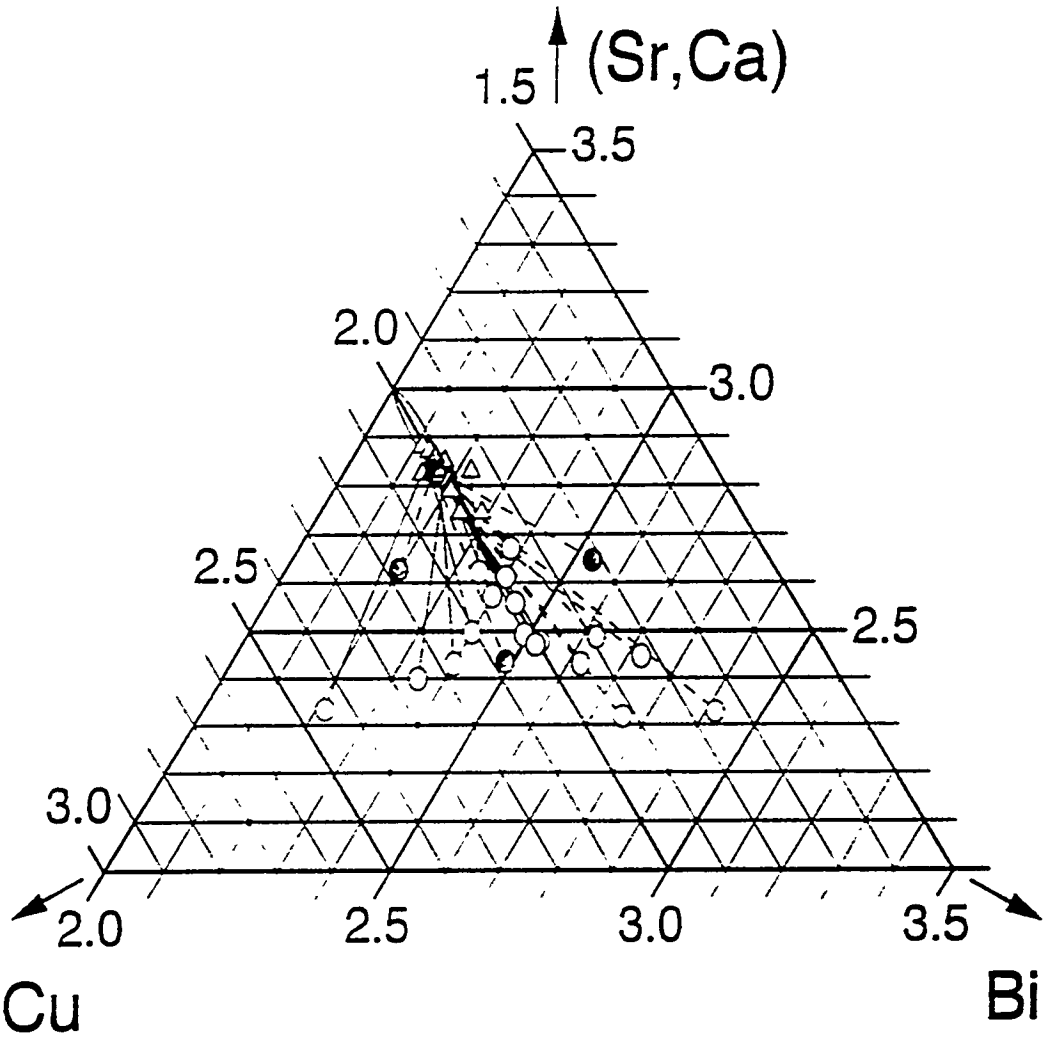

Figure 10: Ternary $Bi_X(Sr,Ca)_YCu_ZO_n$ representation of crystal and melt compositions. The various symbols have the same meaning as in Figure 11.

This contradicts the conclusion of Golden et al., [2] but is not unreasonable considering the nature of the experiments performed.

Golden et al.'s thin films were crystallized by first rapidly melting the mixed components, then allowing them to crystallize. They were also homogenized at elevated temperatures for extended (> 2 hours) times. The

2212 thin films may thus have started as the first solid to crystallize from the melt. They may then have been transformed to single phase films of the original melt composition through later subsolidus annealing processes. The results of our study and that of Golden et al. can thus be viewed as complimentary.

Figure 10 allows one to consider the case of CuO segregation on a ternary section by treating (Sr,Ca)O as a single component. Since SrO and CaO have similar chemistry, this is the most valid technique for describing the BSCCO system as pseudo-ternary. The CuO segregation coefficient is shown to vary about unity in this figure. One may also observe that the CuO content of the 2212 crystals deviates significantly from Ono's assumption that the copper coefficient will always be exactly 2.0. [1]

Both figures show that the more careful composition measurements of Hong et al.[3] resulted in the closest fit between their solubility range and the compositions of inclusion-free 2212 crystals.

(b.) Comparison with bulk crystallization data

The solid and melt compositions measured in the present study may be compared with the earlier crystal growth data listed in Table 1. The present study has produced significantly more data than was previously available. All studies were consistent in finding that 2212 crystals form from melts which are Bi_2O_3-rich and SrO-poor, at temperatures between 820 and 900°C.

Additional crystal growth data was also available from an as-yet unpublished, flux flow study by Lombardo. [4] In this study, 2212 crystals were quenched during growth from melts in MgO crucibles. Microprobe measurements of the as-grown crystals and their melts were then made. This data is compared, in Figures 11 and 12, with the crystal and melt compositions in single-phase LHPG samples.

The $Bi_xSr_yCa_zCu_2O_{8+d}$ representation in Figure 11 shows that Lombardo's crystal and melt compositions are fairly consistent with the float-zone data. The crystals prepared in these experiments had compositions corresponding closely to those of Hong et al. [3] Once again, these crystals were observed to solidify from Bi_2O_3-rich and SrO-poor melts.

The $Bi_x(Sr,Ca)_yCu_zO_{8+d}$ representation in Figure 12 shows the close agreement between the Hong solubility data and Lombardo's crystal

compositions. This figure shows graphically that the copper content in the latter's crystals was greater than that observed in this study. The melts were also lower. Thus, it is possible that different experimental setups can affect the copper oxide segregation coefficient.

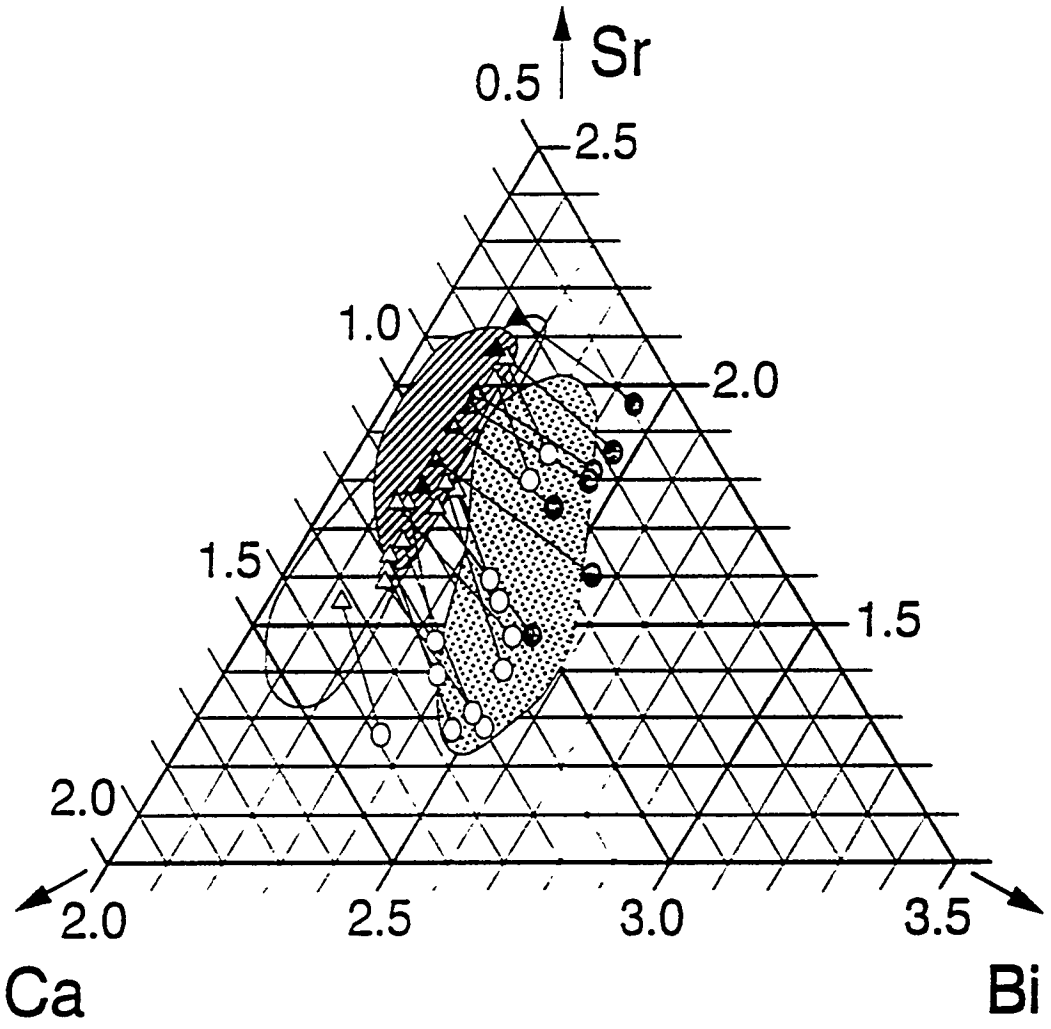

Figure 11 Ternary projection of crystal and melt compositions on the $Bi_xSr_yCa_zCu_2O_{8+d}$ planar section, from LHPG and bulk crystallization [4] studies. White symbols illustrate data from the LHPG experiments, while grey symbols represent compositions from the bulk crystallization study. Otherwise the symbols have the same meaning as before.

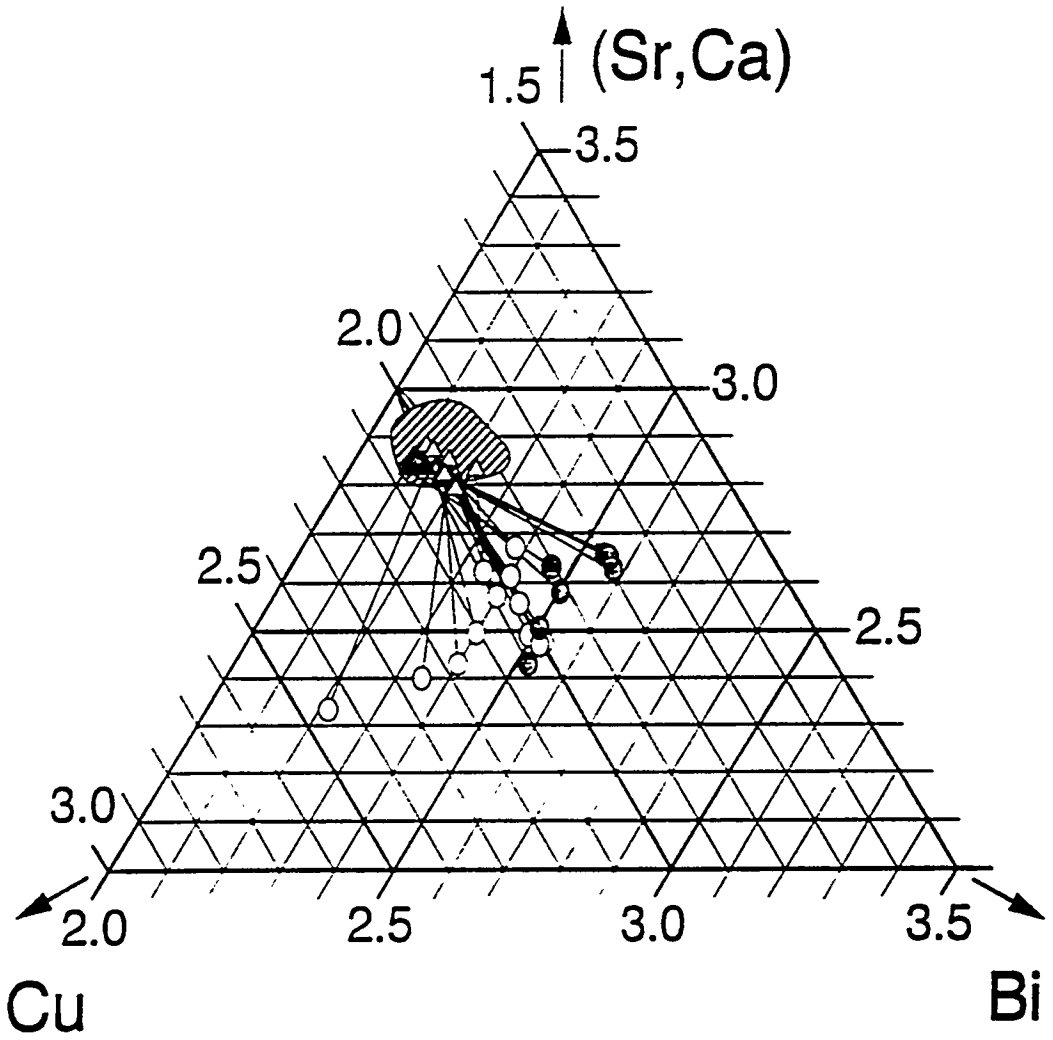

Figure 12: Ternary $Bi_x(Sr,Ca)_yCu_zO_n$ representation of crystal and melt compositions from LHPG and bulk crystallization [7] studies. The symbols have the same meaning as in Figure 11.

(c.) Component Segregation

The segregation behavior of Bi, Ca, Sr and Cu during the float-zone growth of 2212 is compared with that found for the flux growth experiment of Lombardo. [4] Figures 13 through 18 plot the variations in segregation coefficient for the various elements as a function of first, growth temperature, then composition for both sets of experiments. The dark symbols indicate the LHPG data, while open symbols represent the bulk crystallization data.

Figure 13 gives the variation of the bismuth and copper oxide segregation coefficients with observed growth temperature. It shows that, as growth temperature increased, the segregation coefficient of bismuth oxide increased toward unity. The segregation coefficient of copper oxide, meanwhile, decreased with increasing growth temperature. In this case, the segregation coefficient passed through unity (indicating that there was no copper oxide segregation) around 865° C; the middle of the temperature range explored. Combined, these two results clearly show that congruent crystallization of 2212 is not likely in room air because the segregation of both bismuth and copper cannot be simultaneously eliminated.

Similar plots show that the strontium oxide, calcium oxide and (Sr,Ca)O component segregation coefficients did not vary monotonically with observed growth temperature. They also did not vary monotonically with the copper or bismuth oxide contents in the crystals or melts. There was, however, a strong relationship between both the SrO:CaO ratio and the net SrO+CaO content in the melt, and that in the corresponding crystals. This interdependence of the SrO and CaO content is shown in Figures 14 and 15.

The behavior of the copper and bismuth oxide segregation coefficients also showed a striking interdependence. These coefficients are plotted versus bismuth and copper oxide melt composition in Figures 16 and 17. Once again, the bismuth and copper oxide segregation coefficients do not simultaneously approach 1.0 in these plots. It was also apparent that the influence of the bismuth oxide content of the melt on copper oxide segregation differed between the LHPG and flux growth studies. This was the only significant difference observed.

The interrelationship between the Bi, (Sr,Ca), and Cu segregation coefficients for both data sets are summarized in Figure 18. Despite a significant spread in the data, it is still apparent that increased bismuth oxide segregation was accompanied by a decrease in copper oxide segregation in both studies. As before, the (Sr,Ca)O segregation coefficient appeared to be independent of the other system variables.

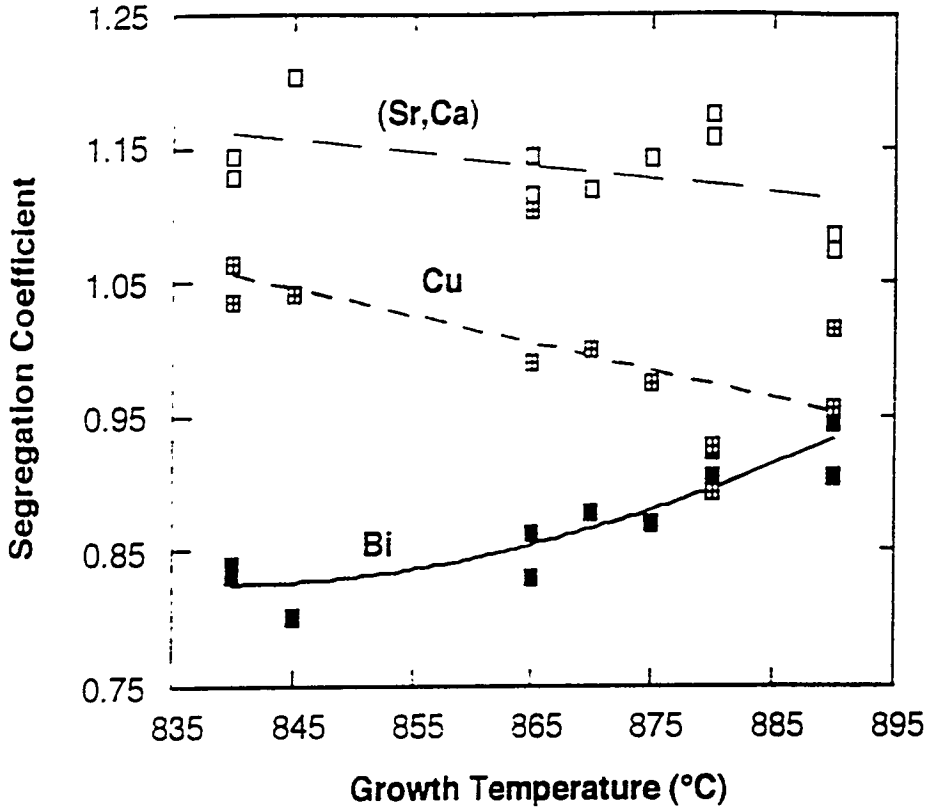

Figure 13: Segregation coefficients, k_{Bi}, $k_{(Sr,Ca)}$, and k_{Cu}, plotted vs. growth temperature.

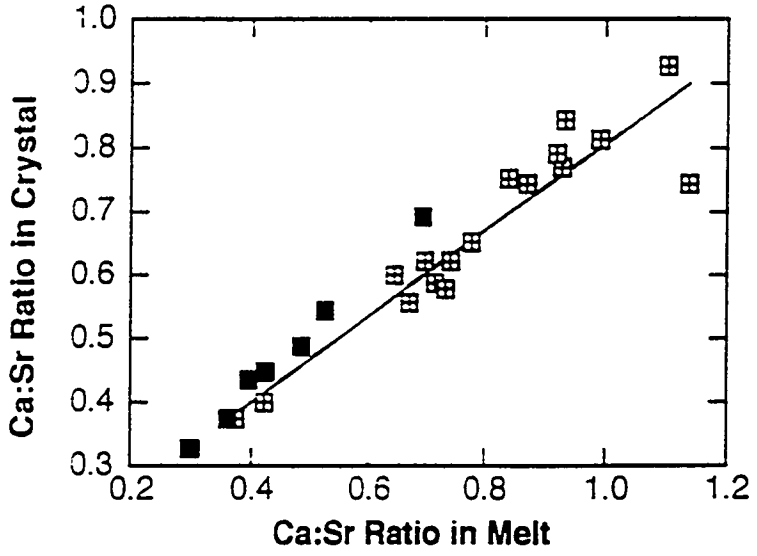

Figure 14: Variation in Ca:Sr ratio in crystal composition, as the Ca:Sr ratio in the melt varies. Results shown for both LHPG and bulk crystallization [4] data

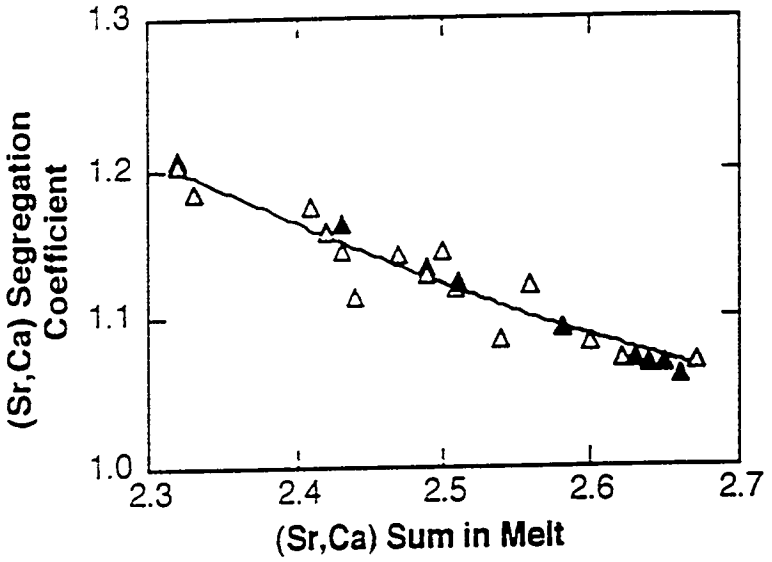

Figure 15: Variation in (Sr,Ca) segregation coefficients as the (Sr,Ca) content of the melt varies. Results shown for both LHPG and bulk crystallization [4] data.

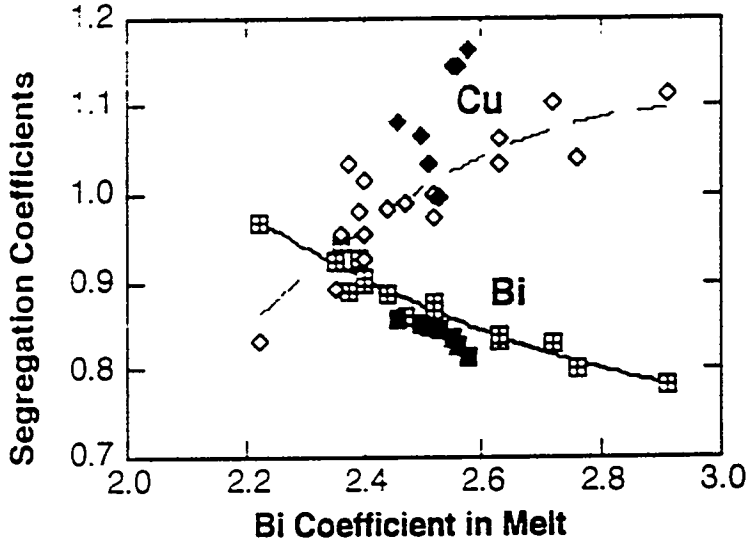

Figure 16: Variation in Bi and Cu segregation coefficients as the Bi content of the melt varies. Results shown for both LHPG and bulk crystallization [4] data.

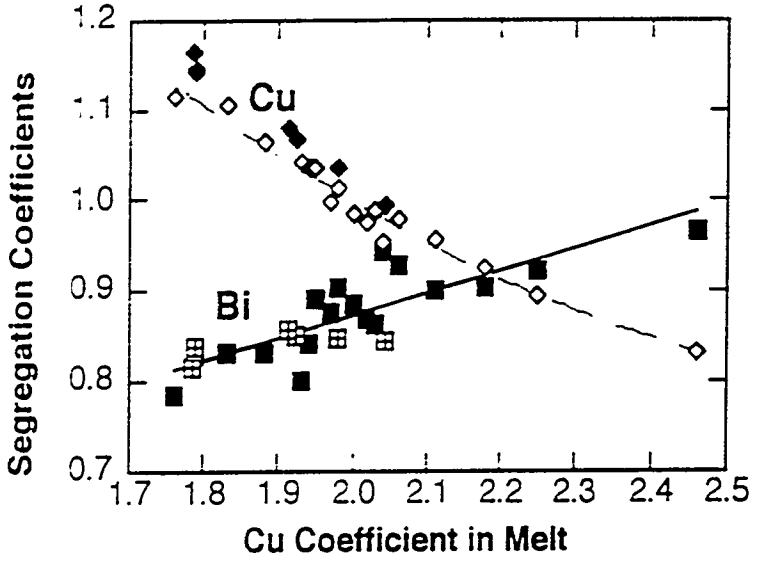

Figure 17: Variation in Bi and Cu segregation coefficients as the Cu content of the melt varies. Results shown for both LHPG and bulk crystallization [4] data.

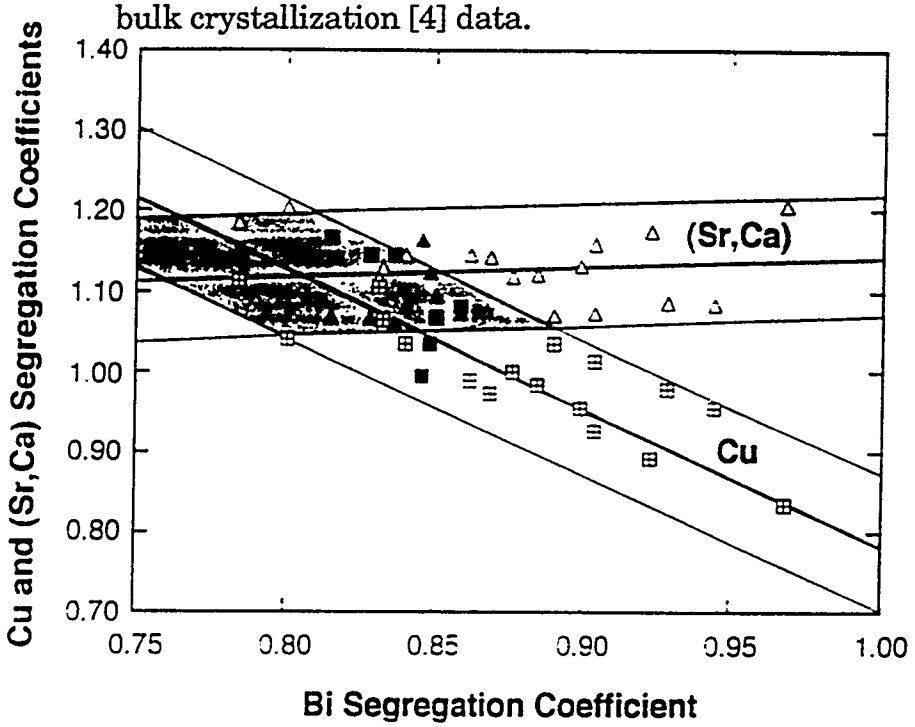

Figure 18: Variation in (Sr,Ca) and Cu segregation coefficients as the Bi segregation coefficient varies. Results shown for both LHPG and bulk crystallization [4] data.

4. Conclusions

While the phase relations in the BSCCO system have been studied by many groups, the temperatures and compositions of the 2212 liquidus and solidus surfaces have not been available. This data is of great importance in designing controlled experiments for the reproducible melt growth of high quality crystals of the 2212 superconductor. The present study produced new data concerning these phase relations by analyzing the crystal and melt compositions, and the growth temperature of miniaturized float-zone samples. These samples were prepared from starting materials having a number of possible 2212 phase compositions.

Comparison between our results and those of other studies shows that our 2212 phase sample compositions formed a subset of the solid solubility ranges reported by Ono [1] and Hong et al. [3] A moderate degree of agreement was also found between our melt (liquidus) compositions and the "2212 solubility range" reported by Golden et al. [2] In addition, the crystal composition, melt composition and crystallization temperature data gathered in this study was observed to be typical of the data available from the flux growth experiments.

As a result of these experiments, a successful technique for the growth of long, single-phase 2212 samples was developed. These experiments showed that such growth was more easily obtained for some starting material compositions, while it was impossible for others. Composition Y ($Bi_{2.1}Sr_{1.8}Ca_{1.1}Cu_2O_y$) was found to produce single-phase material most easily of all the compositions studied.

The growth temperature, crystal composition, and melt composition were identified for a number of single-phase 2212 growth interfaces. These measurements were used to characterize the relevant 2212 crystal/melt equilibrium conditions. It was found that 2212 crystals typically solidify from Bi_2O_3-rich and SrO-poor melts.

The growth temperatures were found to increase with increasing melt concentrations of bismuth and copper oxide. The combined bismuth and copper oxide content of the crystals, however, was found to be relatively invariant. It was thus concluded that component segregation of the bismuth and copper oxide components during 2212 crystallization is interdependent. The copper oxide segregation coefficient was observed to increase above 1.0 as

the bismuth oxide coefficient increased toward 1.0 from below. Based on this analysis, congruent 2212 solidification (in air) does not appear to be possible.

B. ADVANCED FIBER GROWTH STATION

1 History and Background

One of our program goals was to prepare long lengths (> 100 mm) of small diameter (< 100 mm) superconducting fibers under very stable (controlled) growth conditions. Our existing LHPG system was not ideally suited for this application. This fiber growth equipment was originally conceived as a versatile system for exploring a wide variety of materials ranging from 20 μm to 2 mm in diameter. Numerous minor modifications and improvements to its optical and mechanical components were made in order to meet the varying requirements of each individual material. However, because this high T_c superconducting materials program had very specialized requirements, we thought it was important to build a entirely new, more advanced system. One of the major objectives of this program became, therefore, the design and construction of a dedicated fiber growth system capable of routine preparation of 10-50 μm diameter fibers of uniform diameter and in long lengths.

Improvements in laser stability and focusing optics, diameter control, fiber and source rod mounting and guiding, mechanical stability, and the incorporation of motor drive systems with greater precision were identified as essential. Several different approaches were possible in each area, and the design phase involved a thorough evaluation of each alternative to identify those that best met the goals of the program. Since there were only a handful of LHPG systems in the world at the time, and each built by a different group, a proven design did not yet exist. Therefore, we were faced with prioritizing system requirements; modifying existing components, or designing from scratch when our specialized needs could not be met; and integrating the individual components into a complete system.

During the first year of this program studies were undertaken to clarify design concepts and draft a preliminary design. During the second and third years a CO_2 laser was ordered but due to numerous production problems, as mentioned earlier, the initial order had to be cancelled and a new laser company

identified. A laser with superior specifications had become available from United Technologies Optical Systems (UTOS). This newer laser, a commercial version of a military rf-excited single-mode, single-frequency power-stabilized laser, offered twice the power output of the Laser Photonics unit. It was, however, in a pre-production phase but an order was placed early in 1992.

2. Current Year Progress

During the current year the vendor of our new laser system had serious problems with various laser components including the power supply and also stability problems. In the end they were not able to deliver the system to us. Nevertheless work progressed on installing and testing various other components in the LHPG growth station including the computerized fiber translation drive system, the optical train etc. A further no-cost extension was needed, requested and granted.

III. REFERENCES

[1] A. Ono, *Jpn. J. Appl. Phys.* **28**, L1372 (1989).

[2] S. J. Golden, T. E. Bloomer, F. F. Lange, A. M. Segadaes, K. J. Vaidya, and A. K. Cheetham, "Processing and characterization of thin films of the two-layer superconducting phase in the Bi-Sr-Ca-Cu-O system: evidence for solid solution," *J. Amer. Ceram. Soc.* **74**, 123 (1991).

[3] B. Hong and T. O. Mason, *J. Am. Ceram. Soc.* **74**, 1045 (1991).

[4] L. W. Lombardo, private communication.

[5] H. Maeda, Y. Tanaka, N. Fukutomi, and T. Asano, *Jpn. J. Appl. Phys.* **27**, L209 (1988).

[6] R. M. Hazen, C. T. Prewitt, R. J. Angel, N. L. Ross, L. W. Finger, C. G. Hadidiacos, D. R. Veblen,P. J. Heaney, P. H. Hor, R. L. Meng, Y. Y. Sun, Y. Q. Wang, Y. Y. Xue, Z. J. Huang, L. Gao, J. Bechtold, and C. W. Chu, *Phys. Rev. Lett.* **60**, 1174 (1988).

[7] J. M. Tarascon, Y. LePage, P. Barboux, B. G. Bagley, L. H. Green, G. W. Hull, M. Giroud, and D. M. Hwang, *Phys. Rev. B.***37**, 9382 (1988).

[8] T. Schweizer, R. Muller, P. Bohac, and L. J. Gauckler, Proc. of 2nd Intn'l. Ceram. Sci. and Technol. Congress, Orlando, FL (Nov. 1990).

[9] L. L. Lee, J. J. Chen, W. J. Wen, T. P. Perng, J. M. Wu, T. S. Chin, R. S. Liu, and P. T. Wu, *J. Mater. Res.* **5**, 1403 (1990).

[10] S. Takekawa, H. Nozaki, A Umezono, K. Kosuda, and M. Kobayashi, *J. Cryst. Growth* **92**, 687 (1988).

[11] R. S. Feigelson, D. Gazit, D. K. Fork, and T. H. Geballe, *Science* **240**, 1642 (1988).

[12] D. B. Mitzi, L. W. Lombardo, A. Kapitulnik, S. S. Laderman, and R. D. Jacowitz, "Growth and properties of oxygen- and ion-doped $Bi_2Sr_2CaCu_2O_{8+d}$ single crystals," *Phys. Rev. B.* **41**, 6564 (1990).

[13] M. Hikita, T. Iwata, Y. Tajima, and A. Katsui, *J. Cryst. Growth* **91**, 282 (1988).

[14] P. A. Morris, W. A. Bonner, B. G. Bagley, G. W. Hull, N. G. Stoffel, L. H. Greene, B. Meager, and M. Giroud, *Appl. Phys. Lett.* **53**, 249 (1988).

[15] Y. K. Huang, K. Kadowaki, M. J. V. Menken, J. N. Li, K. Bakker, A. A. Menovsky, J. J. M. Franse, G. F. Bastin, H. J. M. Heijligers, H. Barten, J. Van den Berg, R. A. Zacher, and H. W. Zandbergen, *Physica C* **152**, 431 (1988).

[16] M. J. V. Menken, A. J. M. Winkelman, and A. A. Menovsky, *J. Cryst. Growth* **113**, 9 (1991).

[17] M. J. Cima, X. P. Jiang, H. M. Chow, J. S. Haggerty, M. C. Fleming, R. A. Laudise, and D. W. Johnson, *J. Mater. Res.* **5**, 1834(1990).

[18] D. Elwell and H. J. Scheel, *Growth of Crystals form High-temperature Solutions*, Academic Press, NY (1975).

[19] B.C. Chakoumankos, P.S. Ebey, B.C. Sales and E. Sonder, J. Mater.Res. 4, 767 (1989)